JACS
JOURNAL OF THE AMERICAN CHEMICAL SOCIETY
Communication
pubs.acs.org/JACS

Phosphorus-Based Alloy Materials for Advanced Potassium-Ion Battery Anode

Wenchao Zhang,[†,‡,⊥] Jianfeng Mao,[‡,⊥] Sean Li,[§] Zhixin Chen,*[,†] and Zaiping Guo*[,†,‡]

[†]Engineering Materials Institute, School of Mechanical, Materials & Mechatronics Engineering, University of Wollongong, Wollongong, New South Wales 2500, Australia

[‡]Institute for Superconducting & Electronic Materials, University of Wollongong, Wollongong, New South Wales 2522, Australia

[§]School of Materials Science and Engineering, The University of New South Wales, Kensington, New South Wales 2052, Australia

Supporting Information

ABSTRACT: Potassium-ion batteries (PIBs) are interesting as one of the alternative metal-ion battery systems to lithium-ion batteries (LIBs) due to the abundance and low cost of potassium. We have herein investigated Sn_4P_3/C composite as a novel anode material for PIBs. The electrode delivered a reversible capacity of 384.8 mA h g^{-1} at 50 mA g^{-1} and a good rate capability of 221.9 mA h g^{-1}, even at 1 A g^{-1}. Its electrochemical performance is better than any anode material reported so far for PIBs. It was also found that the Sn_4P_3/C electrode displays a discharge potential plateau of 0.1 V in PIBs, slightly higher than for sodium-ion batteries (SIBs) (0.01 V), and well above the plating potential of metal. This diminishes the formation of dendrites during cycling, and thus Sn_4P_3 is a relatively safe anode material, especially for application in large-scale energy storage, where large amounts of electrode materials are used. Furthermore, a possible reaction mechanism of the Sn_4P_3/C composite as PIB anode is proposed. This work may open up a new avenue for further development of alloy-based anodes with high capacity and long cycle life for PIBs.

The demand for energy storage materials is high and increasing with the rapid development of electronic devices, electric vehicles, and large-scale energy storage system (ESS).[1−4] The widespread use of lithium-ion batteries (LIBs) for these applications is seriously limited by the uneven distribution and the short supplies of lithium minerals (0.0017 wt %) around the world.[5] Sodium-ion batteries (SIBs) have recently attracted increasing interest due to the natural abundance of sodium.[6−8] Unfortunately, their relatively high standard hydrogen potential (−2.71 V vs $E°$) compared to LIBs (−3.04 V vs $E°$) makes the energy density of SIBs relatively low and limits their potential industrial applications.[6,9−11]

Considering the similar positions of Li, Na, and K in the periodic table and the natural abundance of potassium,[12−16] the potassium-ion battery (PIB) system could be considered as well. Because the standard hydrogen potential of K (−2.93 V vs $E°$) is lower than that of Na and closer to that of Li, PIBs have potential as low-cost batteries with high energy density and high voltage.[17−20] Nevertheless, it is challenge to develop suitable electrodes to accommodate the large size of the K-ions (1.38 Å) compared to Na-ions and Li-ions. Carbonaceous materials have been investigated as PIB anodes, although the highest reported capacity is 273 mA h g^{-1} for soft carbon at C/40.[13]

Although there have been few investigations of alloy-based anode materials in PIBs, an investigation of Sn/C composite anode in a PIB was recently reported, which delivered only 150 mA h g^{-1} after 30 cycles at a current density of 25 mA g^{-1},[21] not much better than for carbon anode materials. Phosphorus (P) has a high theoretical capacity of 2594 mA h g^{-1} because it can form K_3P, a binary phase with K.[22]

Herein, we have investigated the electrochemical performance of P/C and Sn_4P_3/C composites as anode materials for PIBs. The P/C anode delivered a high capacity, but it decayed very fast. In contrast, the Sn_4P_3/C electrode delivered a reversible capacity of 384.8 mA h g^{-1} at a current density of 50 mA g^{-1} and good rate capability of 221.9 mA h g^{-1}, even at a current density of 1 A g^{-1}, the best electrochemical performance reported so far for any anode material for PIBs. Moreover, the reduction potential of the Sn_4P_3 electrode in the PIBs was measured to be 0.1 V, higher than its 0.01 V in SIBs. The K-alloy reactions thus occur at a higher potential than the Na-alloy reactions, so that the PIBs with the Sn_4P_3/C electrode will have a lower risk of short-circuiting due to dendrite growth.

Figure 1a shows the X-ray diffraction (XRD) patterns of the as-prepared Sn_4P_3/C, Sn/C, and P/C powders ball milled under the same conditions. All the diffraction peaks in the XRD pattern of the Sn_4P_3/C composite and the as-prepared sample is virtually pure Sn_4P_3 (ICSD No. 15014). Figure 1b−i displays field-emission scanning electron microscopy (FESEM) and transmission electron microscopy (TEM) images of the Sn_4P_3/C powder. The powder mainly consists of irregular agglomerated micrometer sized particles, as shown in Figure 1b. The agglomerated microparticles consist of many crystalline nanoparticles around 20−50 nm, distributed evenly in the amorphous carbon matrix (Figure 1c,d). Figure 1d shows the lattice fringes of the (107) planes of Sn_4P_3, and the spacing of the fringes is 0.283 nm, which matches the d_{107} spacing of Sn_4P_3. The selected area electron diffraction (SAED) pattern and high resolution TEM (HRTEM) image clearly demonstrate that the Sn_4P_3 nanoparticles are uniformly distributed in the amorphous carbon matrix, which could act as a buffer to

Received: December 1, 2016
Published: February 17, 2017

DOI: 10.1021/jacs.6b12185
J. Am. Chem. Soc. 2017, 139, 3316−3319

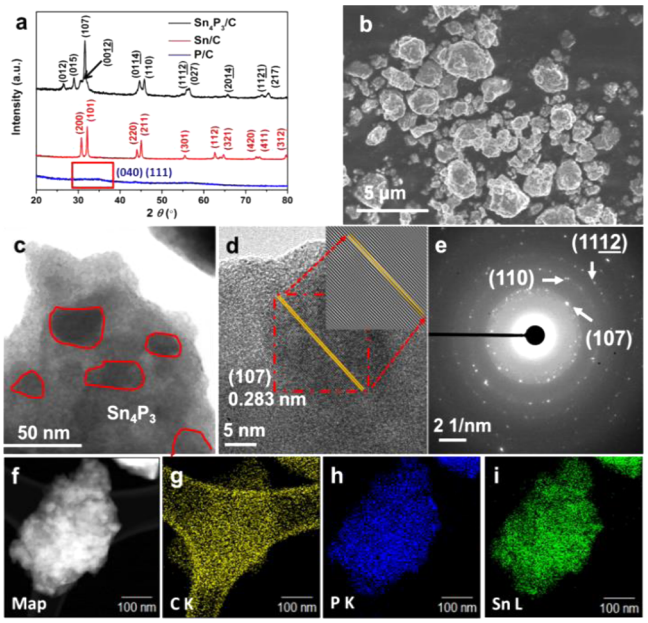

Figure 1. Characterization of Sn_4P_3/C powder: (a) XRD pattern compared with Sn/C and P/C, (b) FESEM image, (c) TEM image, with the red outlines indicating the Sn_4P_3 nanoparticles, (d) HRTEM image and FFT pattern of the red area (inset), (e) SAED pattern, and (f–i) EDS maps of Sn_4P_3/C powder.

suppress the volume changes during the potassiation/depotassiation. Figure 1f–i presents energy dispersive spectroscopy (EDS) elemental mapping images of a nano-Sn_4P_3 particle with uniform distributions of the Sn, P, and C.

The K-ion storage behavior of the Sn_4P_3/C electrode was investigated by cyclic voltammetry (CV) and compared with its performance in SIBs (Figure 2a,b). For the PIBs (Figure 2a) a major peak at around 0.01 V was observed in the initial cathodic scan. During the subsequent cycles, this large reduction band was shifted to 0.1 V. In the anodic scan, two oxidation bands centered at 0.8 and 1.15 V due to the depotassiation processes of K–Sn and K–P can be observed. The lowest reduction peak for the Sn_4P_3/C electrode (Figure 2b) is at 0.1 V versus K^+/K and 0.01 V versus Na^+/Na, respectively. Considering the fact that dendrite formation becomes more serious when the reduction potential is close to the plating potential, PIBs could be safer than SIBs when using Sn_4P_3 as anode. The discharge and charge profiles of the Sn_4P_3/C electrodes for PIBs and SIBs are compared and shown in Figure 2c,d. The discharge slopes for the Sn_4P_3/C electrode are around 0.1–0.6 V for the PIBs and 0.01–0.5 V for the SIBs, respectively.

Figure 2e displays the cycling performances of the Sn_4P_3/C, P/C, and Sn/C electrodes in PIBs at the current density of 50 mA g^{-1}. The first discharge capacity of the Sn_4P_3/C electrode (588.7 mA h g^{-1}) is higher than that of the Sn/C (358.2 mA h g^{-1}) but lower than that of the P/C (2171.7 mA h g^{-1}). The P/C and Sn/C electrodes only managed to retain 9% and 20%, respectively, of their reversible capacity after 20 cycles. In contrast, the Sn_4P_3/C electrode shows much better cycling performance compared with the P/C and Sn/C electrodes, where the capacity increased gradually up to 30 cycles and faded gradually after that. Nevertheless, the Sn_4P_3/C electrode still retained the capacity of 307.2 mA h g^{-1} after 50 cycles,

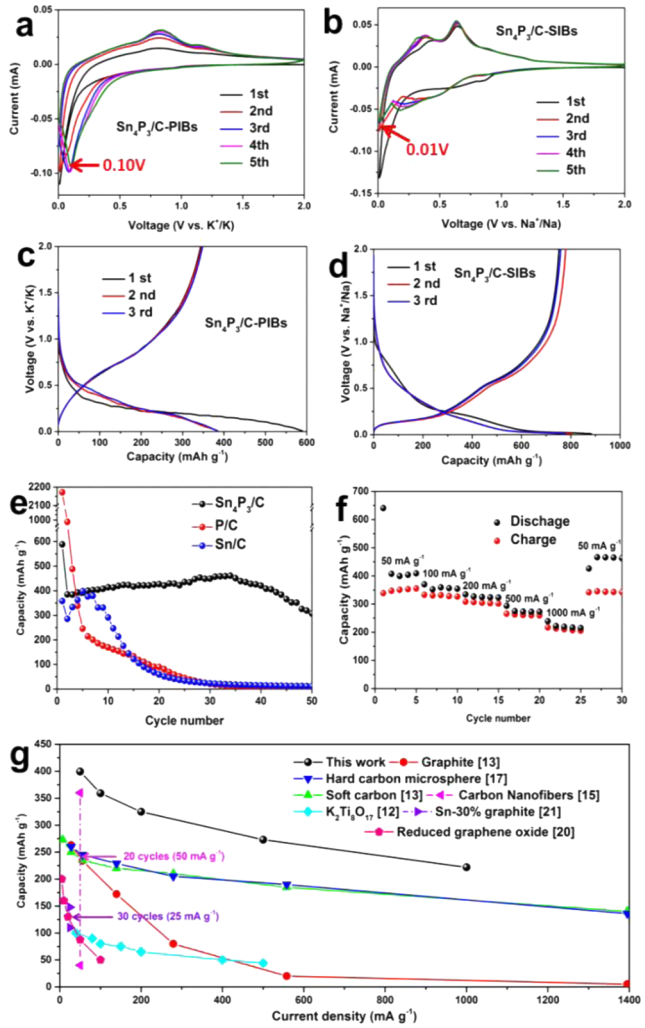

Figure 2. Cyclic voltammograms (CVs) for the first 5 cycles of (a) Sn_4P_3/C in PIBs and (b) Sn_4P_3/C in SIBs at the scanning rate of 0.05 mV s^{-1}. The initial, second, and third discharge/charge profiles of (c) Sn_4P_3/C in PIBs and (d) Sn_4P_3/C in SIBs at the current density of 50 mA g^{-1}. (e) Cycling performance of the Sn_4P_3/C, Sn/C, and P/C electrodes in PIBs at the current density of 50 mA g^{-1}. (f) Rate performance of Sn_4P_3/C electrode in PIBs at various current densities from 50 to 1000 mA g^{-1}. (g) Rate capacities of the Sn_4P_3/C anode and the other reported anodes in PIBs.

which is almost 80% of its reversible capacity. Long-term cycling performance was displayed in Figure S7.

TEM and SEM were carried out on the cycled samples to show the morphology and microstructure changes, as shown in Figures S9 and S10 in the Supporting Information, respectively. The nano-Sn_4P_3 particles are still intact in the crystalline state (Figure S9) but become smaller in size (5–8 nm) after 30 cycles. Their even distribution within the carbon matrix provides effective electrode/electrolyte contact, short ionic diffusion paths, and improved reaction kinetics,[23] so that they contribute to the gradual capacity rise before the 30th cycle. After the 50th cycle, the original crystalline particles were decrystallized and agglomerated into larger globules, and the cracks in the Sn_4P_3/C electrode become much bigger during the cycling process (Figure S10), mostly after 30 cycles, indicating large strain caused by large volume changes in the Sn_4P_3 electrode during cycling, and loss of integrity of the

DOI: 10.1021/jacs.6b12185
J. Am. Chem. Soc. 2017, 139, 3316–3319

electrode due to particle pulverization leads to decreased capacity.

The rate capability of the Sn_4P_3/C electrode in PIBs was also characterized, as shown in Figure 2f. The potassiation capacity decreased from 399.4 to 221.9 mA h g^{-1} when the current density increased from 50 to 1000 mA g^{-1}. The rate capacities of all the reported anodes used in PIBs (graphite, soft carbon,[13] hard carbon microsphere,[17] carbon nanofibers,[15] Sn/C composite,[21] reduced graphene oxide,[20] and $K_2Ti_8O_{17}$[12]) are presented in Figure 2g. It is clear that the rate capability of the Sn_4P_3/C electrode is the best among the reported anode materials.

To understand the possible reaction mechanisms during the discharge and charge processes, ex-situ XRD was used to identify the possible phases. As shown in Figure 3a, after the

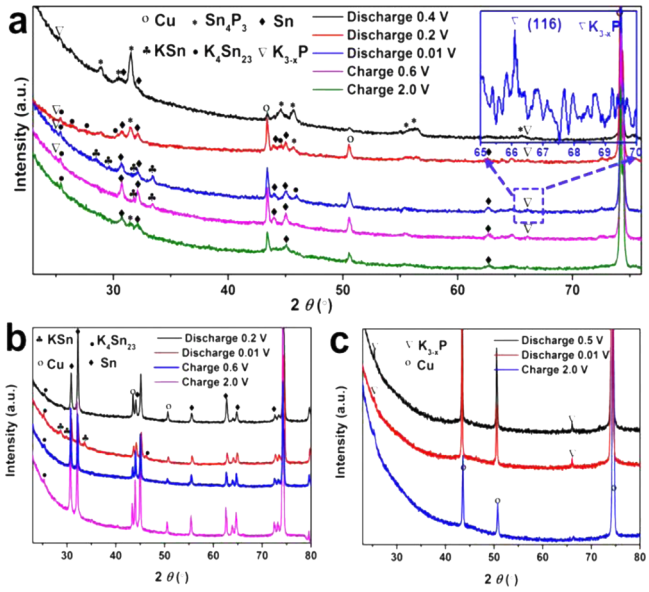

Figure 3. Ex-situ XRD patterns of cycled (a) Sn_4P_3/C and enlarged area (65°–70°) at 0.01 V at discharged potential (inset), (b) Sn/C, and (c) P/C electrodes in PIBs at different potentials.

Sn_4P_3/C electrode was discharged to 0.4 V, XRD signals from the Sn_4P_3 electrode decreased notably, and XRD signals from $K_{3-x}P$ could be detected. When the Sn_4P_3/C electrode was further discharged to 0.2 V, Sn phase appeared and became the main phase at the expense of the Sn_4P_3, indicating a conversion reaction. Meanwhile, several new peaks of K_4Sn_{23} (ICSD No. 25301) were observed. After the Sn_4P_3/C electrode was discharged to 0.01 V, KSn phase (ICSD No. 409435) and minor Sn peaks could be detected, indicating the alloying of potassium with tin. The same results were also obtained in the Sn/C anode, where K_4Sn_{23} and KSn phases were also observed after discharging to 0.2 and 0.01 V, as shown in Figure 3b. It is well-known that the binary K–P system has the following phases: KP (ICSD No. 14010), K_4P_3 (ICSD No. 64625), K_3P_{11} (ICSD No. 36590), and K_3P (ICSD No. 25550).[22] As for the cycled P/C electrodes, which were discharged to 0.5 or 0.01 V (Figure 3c), two new peaks in addition to the peaks of copper were detected at 25.38° and 65.91°, which correspond to the (102) and (116) of the layered structured K_3P phase with space group $P6_3/mmc$ (Figure S11). The strongest peak of K_3P is missing, possibly due to partial potassiation, so the final discharge product could be a nonstoichiometric $K_{3-x}P$ compound or amorphous. On the basis of this discussion, we postulate that KSn and $K_{3-x}P$ are the two possible final products after the discharge of the Sn_4P_3/C electrode in PIBs, with the theoretical capacity of Sn_4P_3 as high as 620 mA h g^{-1}, which is more than 2 times the capacity of carbon anode materials. In the charging process, a new peak at 31.4° was detected after charging to 2.0 V, representing the reformation of the Sn_4P_3. Therefore, the potassiation/depotassiation of Sn_4P_3 via conversion and alloying reactions is partially reversible. The reaction mechanism of Sn_4P_3 as anode material for SIBs was previously thoroughly investigated, and in some cases, the Sn_4P_3 phase was found to be restored as well, even after desodiation at 1.5 V.[24] Accordingly, the potassiation and depotassiation mechanism may be described by the following equations:

$$Sn_4P_3 + (9 - 3x)K \leftrightarrow 4Sn + 3K_{3-x}P \quad (1)$$

$$23Sn + 4K \leftrightarrow K_4Sn_{23} \quad (2)$$

$$K_4Sn_{23} + 19K \leftrightarrow 23KSn \quad (3)$$

The superior electrochemical performance of the Sn_4P_3/C composite compared to Sn/C and P/C can be first understood from the active nature of the Sn_4P_3 itself, where the Sn and P components in the Sn_4P_3/C are combined to give a synergistic K-storage reaction. The reaction mechanism of Sn_4P_3 during potassiation/depotassiation is schematically shown in Scheme 1. Upon potassiation, a conversion reaction first occurs, where the Sn_4P_3 breaks into small Sn particles and a $K_{3-x}P$ matrix

Scheme 1. Potassiation/Depotassiation Process in Sn_4P_3/C Electrode

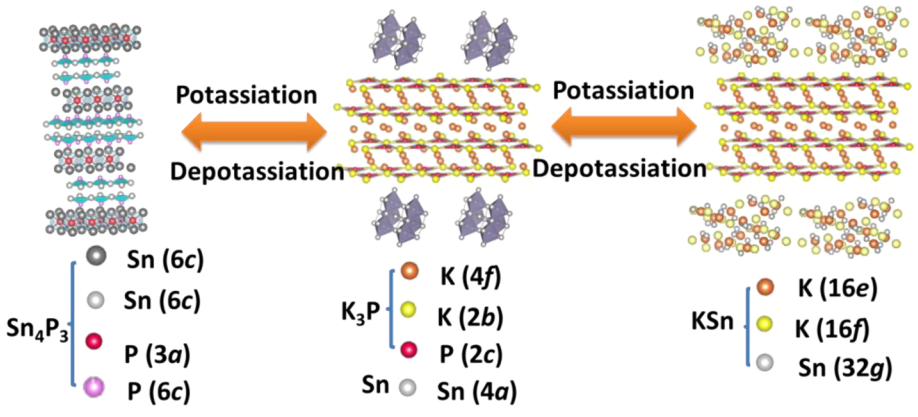

DOI: 10.1021/jacs.6b12185
J. Am. Chem. Soc. 2017, 139, 3316–3319

(Reaction 1). Upon further potassiation, K is inserted into Sn to first form K_4Sn_{23} (Reaction 2) and finally KSn (Reaction 3) through the alloying reaction. During the depotassiation, KSn dealloys first to form Sn, and then the Sn reacts with $K_{3-x}P$ to convert it back to Sn_4P_3. Thus, the stepped formation of K−Sn (K_4Sn_{23}, KSn) and K−P alloy ($K_{3-x}P$) phases during the discharge process creates mutual buffers to alleviate the volume changes during cycling. The conductive carbon matrix provides a further buffering effect against volume changes during cycling, thus maintaining the integrity of the electrode and enhancing the electrical conductivity, leading to improved cycling stability of the electrode.

In summary, Sn_4P_3/C composite, introduced for the first time as an anode material for the potassium-ion battery, was synthesized by a conventional and scalable ball-milling technique. Compared with Sn_4P_3/C in SIBs, Sn_4P_3/C electrode in PIBs could deliver a discharge voltage plateau (0.1 V) that is low enough for an anode, but slightly higher than the plating potential of the corresponding metal (0.01 V), thus avoiding the formation of dendrites and improving the safety of the battery. Our investigation of the reaction mechanisms of the Sn_4P_3 indicates that K−Sn (K_4Sn_{23}, KSn) and K−P alloy ($K_{3-x}P$) phases are formed during the discharge process, with these phases acting as mutual buffers to alleviate the volume changes during cycling. The conductive carbon matrix enhances the electrical conductivity of the electrode and works as a buffer matrix to accommodate the volume changes in the active materials during cycling, maintaining the integrity of the electrode and the cycle life. This work may help in the search for a safe, high-energy-density, and low-cost rechargeable K-ion battery for large-scale energy storage applications.

■ ASSOCIATED CONTENT

Supporting Information

The Supporting Information is available free of charge on the ACS Publications website at DOI: 10.1021/jacs.6b12185.

Experimental section; additional data from Raman spectroscopy, XPS of Sn_4P_3/C, SEM, CV curves, discharge−charge profiles of Sn/C and P/C, XRD, Raman and electrochemical results for bare Sn_4P_3, ex-situ TEM and SEM images of Sn_4P_3/C electrode after cycling, enlarged ex-situ results, ex-situ EDS maps and diffraction patterns, cycling performance with different voltage ranges, crystallography data on K_3P phase (PDF)

■ AUTHOR INFORMATION

Corresponding Authors

*zchen@uow.edu.au

*zguo@uow.edu.au

ORCID

Zaiping Guo: 0000-0003-3464-5301

Author Contributions

⊥These authors contributed equally.

Notes

The authors declare no competing financial interest.

■ ACKNOWLEDGMENTS

The authors acknowledge the financial support from the Australian Research Council (ARC) through an ARC Discovery Project (DP170102406) and the facilities in the Electron Microscopy Centre of the University of Wollongong (UOW), with special thanks to Dr. Wei Kong Pang for the analysis of ex-situ XRD results, Ms. Yajie Liu for Raman tests and Dr. Tania Silver for editing. Wenchao Zhang thanks the UOW and Engineering Materials Institute of UOW for financial support.

■ REFERENCES

(1) Dubal, D. P.; Ayyad, O.; Ruiz, V.; Gomez-Romero, P. *Chem. Soc. Rev.* **2015**, *44*, 1777.

(2) Larcher, D.; Tarascon, J. *Nat. Chem.* **2015**, *7*, 19.

(3) Xie, Y.; Naguib, M.; Mochalin, V. N.; Barsoum, M. W.; Gogotsi, Y.; Yu, X.; Nam, K.-W.; Yang, X.-Q.; Kolesnikov, A. I.; Kent, P. R. *J. Am. Chem. Soc.* **2014**, *136*, 6385.

(4) Wu, F.; Xing, Y.; Zeng, X.; Yuan, Y.; Zhang, X.; Shahbazian-Yassar, R.; Wen, J.; Miller, D. J.; Li, L.; Chen, R.; Lu, J.; Amine, K. *Adv. Funct. Mater.* **2016**, *26*, 7626.

(5) Goodenough, J. B.; Park, K.-S. *J. Am. Chem. Soc.* **2013**, *135*, 1167.

(6) Yabuuchi, N.; Kubota, K.; Dahbi, M.; Komaba, S. *Chem. Rev.* **2014**, *114*, 11636.

(7) Dahbi, M.; Yabuuchi, N.; Kubota, K.; Tokiwa, K.; Komaba, S. *Phys. Chem. Chem. Phys.* **2014**, *16*, 15007.

(8) Chen, C.; Wen, Y.; Hu, X.; Ji, X.; Yan, M.; Mai, L.; Hu, P.; Shan, B.; Huang, Y. *Nat. Commun.* **2015**, *6*, 6929.

(9) Kundu, D.; Talaie, E.; Duffort, V.; Nazar, L. F. *Angew. Chem., Int. Ed.* **2015**, *54*, 3431.

(10) Palomares, V.; Casas-Cabanas, M.; Castillo-Martínez, E.; Han, M. H.; Rojo, T. *Energy Environ. Sci.* **2013**, *6*, 2312.

(11) Hong, S. Y.; Kim, Y.; Park, Y.; Choi, A.; Choi, N.-S.; Lee, K. T. *Energy Environ. Sci.* **2013**, *6*, 2067.

(12) Han, J.; Xu, M.; Niu, Y.; Li, G.-N.; Wang, M.; Zhang, Y.; Jia, M.; Li, C. m. *Chem. Commun.* **2016**, *52*, 11274.

(13) Jian, Z.; Luo, W.; Ji, X. *J. Am. Chem. Soc.* **2015**, *137*, 11566.

(14) Zhao, Q.; Wang, J.; Lu, Y.; Li, Y.; Liang, G.; Chen, J. *Angew. Chem.* **2016**, *128*, 12716.

(15) Liu, Y.; Fan, F.; Wang, J.; Liu, Y.; Chen, H.; Jungjohann, K. L.; Xu, Y.; Zhu, Y.; Bigio, D.; Zhu, T.; Wang, C. *Nano Lett.* **2014**, *14*, 3445.

(16) Wessells, C. D.; Peddada, S. V.; Huggins, R. A.; Cui, Y. *Nano Lett.* **2011**, *11*, 5421.

(17) Jian, Z.; Xing, Z.; Bommier, C.; Li, Z.; Ji, X. *Adv. Energy Mater.* **2016**, *6*, 1501874.

(18) Eftekhari, A.; Jian, Z.; Ji, X. *ACS Appl. Mater. Interfaces* **2017**, *9*, 4404.

(19) Zhao, J.; Zou, X.; Zhu, Y.; Xu, Y.; Wang, C. *Adv. Funct. Mater.* **2016**, *26*, 8103.

(20) Luo, W.; Wan, J.; Ozdemir, B.; Bao, W.; Chen, Y.; Dai, J.; Lin, H.; Xu, Y.; Gu, F.; Barone, V.; Hu, L. *Nano Lett.* **2015**, *15*, 7671.

(21) Sultana, I.; Ramireddy, T.; Rahman, M. M.; Chen, Y.; Glushenkov, A. M. *Chem. Commun.* **2016**, *52*, 9279.

(22) Sangster, J. M. *J. Phase Equilib. Diffus.* **2010**, *31*, 68.

(23) Li, X.; Rui, M.; Song, J.; Shen, Z.; Zeng, H. *Adv. Funct. Mater.* **2015**, *25*, 4929.

(24) Mao, J.; Fan, X.; Luo, C.; Wang, C. *ACS Appl. Mater. Interfaces* **2016**, *8*, 7147.

DOI: 10.1021/jacs.6b12185
J. Am. Chem. Soc. 2017, 139, 3316−3319